8-27-2020

Divergence of the dielectric constant in ultrathin granular metal films near the percolation threshold

H. Bakkali

E. Blanco

Samuel Lofland
Rowan University, lofland@rowan.edu

M. Dominguez

Recommended Citation

Bakkali, H., Blanco, E., Lofland, S.E. & Dominguez, M. (2020). Divergence of the dielectric constant in ultrathin granular metal films near the percolation threshold. New Journal of Physics 22, 083018.

PAPER • OPEN ACCESS

Divergence of the dielectric constant in ultrathin granular metal films near the percolation threshold

To cite this article: H Bakkali *et al* 2020 *New J. Phys.* **22** 083018

New Journal of Physics
The open access journal at the forefront of physics

Deutsche Physikalische Gesellschaft DPG
IOP Institute of Physics

Published in partnership with: Deutsche Physikalische Gesellschaft and the Institute of Physics

OPEN ACCESS

RECEIVED
25 February 2020

REVISED
25 May 2020

ACCEPTED FOR PUBLICATION
25 June 2020

PUBLISHED
7 August 2020

PAPER

Divergence of the dielectric constant in ultrathin granular metal films near the percolation threshold

H Bakkali[1,2], E Blanco[2], S E Lofland[1,3] and M Domínguez[2]

[1] Department of Physics and Astronomy, Rowan University, 201 Mullica Hill Road, Glassboro, NJ 08028, United States of America
[2] Departamento de Física de la Materia Condensada & IMEYMAT: Institute of Research on Electron Microscopy and Materials, University of Cadiz, E11510 Puerto Real, Cádiz, Spain
[3] Author to whom any correspondence should be addressed.

E-mail: lofland@rowan.edu

Keywords: percolation, tunneling conduction, optical conductivity

Abstract

We report on the electronic and optical properties of ultrathin granular films. We demonstrate that the static dielectric constant increases with thickness in the dielectric regime and diverges at the critical thickness, as predicted by classical percolation theory. However, for thicker samples, the dc conductivity does not obey scaling laws due to the presence of tunneling conduction. In this region the dielectric constant is positive, and the electronic transport is not metallic but can be described by Jonscher's universal power law, even though there is a Drude-like response indicating the presence of free charge carriers. Only for thicker films when the dielectric constant becomes negative is there metallic conduction.

Granular metals consisting of metal nanoparticles randomly distributed in an insulating matrix have received particular interest in the research field of modern condensed matter physics due to their fascinating electrical, magnetic and optical properties [1–7]. For example, granular metals have attracted significant interest as engineered plasmonic metamaterials [8, 9], and for photocatalysis [10] and microwave applications [11]. On the other hand, these materials are of importance for studying quantum effects and electronic correlation effects [12–14].

Granular metals may exhibit weak coupling ($g < 1$) or strong coupling ($g > 1$) [15], where $g = h/[4e^2R_t(T \to \infty)]$ is the dimensionless tunnel conductance, with h Planck's constant, e the elementary charge and $R_t(T \to \infty)$ asymptotic tunnel resistance at high temperature [16]. Near the percolation threshold, the volume fraction x of the metal plays a key role in governing the electronic transport with regimes ranging from thermally activated electron tunneling to metallic [2, 4, 17, 18]. The change in interparticle electron transfer is manifested when x reaches a critical value x_c. In the dielectric (weak-coupling) regime when $x \ll x_c$ most of the particles are isolated, and it has been shown that the electronic transport occurs by tunneling of electrons which are linked to adjacent particles separated by a typical tunneling distance < 1 nm [6, 19]. Percolating gold films exhibit a meandering and ramified morphology and their electronic properties can be described by different models such as the regular array of cells, the co-tunneling model, and the conduction-percolation model [20]. In the regular array of cells model, the effective resistance $R_{\rm eff}$ of the gold island array can be expressed as $R_{\rm eff} = R_{\rm Au} + R_{\rm t}$ where $R_{\rm Au}$ is the ohmic resistance of a single gold island and $R_{\rm t}$ the tunnel resistance of a single junction. It is reported that when island coalescence increases, the length l of its meandering structure increases, while the average width and thickness of the meanders essentially stay unchanged [21]. Consequently, as the film coalesces, the tunnel junctions disappear and, although $R_{\rm Au}$ increases as l increases, R dramatically decreases since parallel electron transport pathways appear. In contrast, in the dielectric regime, it has been recently shown [5] that Jonscher's universal power law (JUPL) [22] holds for the ac conductance, but a complete description of the electronic transport in granular metals has yet to be reported.

Theoretical and computational models [23–26] have shown that the physical properties of percolating systems deal with scaling laws which are sensitive only to dimensionality. They predict scaling behavior for

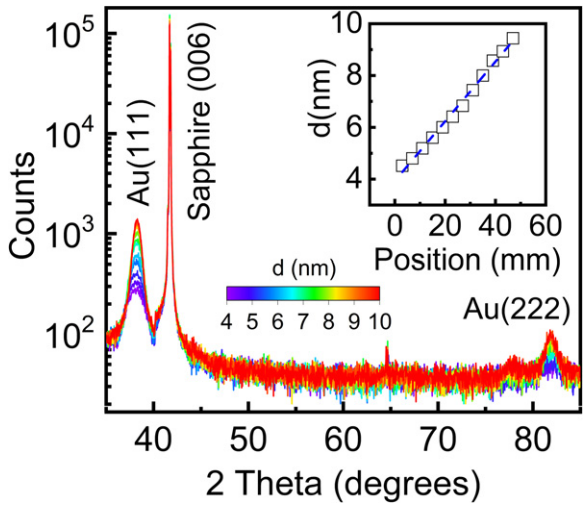

Figure 1. X-ray diffraction patterns obtained at different positions on the substrate. Aside from the (111) reflection of Au, only the *c*-axis reflections from the substrate are observed. Inset shows the dependence of nanocrystallite size *d* as a function of position. A linear fit to the data yielded a gradient for the nanocrystallite size of 1.1 Å mm^{-1}.

both the real part of the static dielectric constant $\varepsilon_1(0)$ and the dc conductivity σ_{dc} near the percolation threshold:

$$\varepsilon_1(0) \propto |t - t_c|^{-s} \tag{1}$$

for $t < t_c$ and

$$\sigma_{dc} \propto (t - t_c)^q \tag{2}$$

for $t > t_c$ where t is the thickness and t_c the critical thickness. Efros and Shklovskii [24] predicted $s = 1.3$ and $s = 1$ for two-dimensional and three-dimensional systems, respectively, and criticality has been observed in some percolating systems [27–34]. On the other hand, Schwartzkopf *et al* [35] proposed a geometrical model of cluster growth in which they assume uniform hemispherical clusters of radius R arranged in a two-dimensional hexagonal lattice with a distance D between the lattice points, where D is the mean cluster correlation distances. They demonstrated that

$$R = \sqrt[3]{\frac{3^{3/2}}{4\pi} D^2 t}. \tag{3}$$

Accordingly, when $D = 2R$, clusters start to interconnect and form a conductive pathway over the macroscopic sample area. This corresponds to the percolation threshold [36] for which, in the case of gold, 3.5×10^{11} clusters cm^{-2} composed of approximately $(1.25 \pm 0.21) \times 10^5$ atoms impinge on each other according to this model while only 6% of the gold atoms on the surface of the clusters.

Hövel *et al* [29, 30], showed that in a set of granular Au thin films, the zero crossing of $\varepsilon_1(0)$ occurred at the metal-to-dielectric transition at a thickness of 6.7 nm which was slightly larger than the critical thickness of 6.4 nm. While they pointed out that the onset of the metallic conductivity may lead to negative values of $\varepsilon_1(0)$, they did not clearly observe a region below t_c where the positive values of $\varepsilon_1(0)$ decreased with thickness in the tunneling conduction (TC) regime. However, if the divergent region were rather narrow, it may have easily been missed in a set of films with discrete thicknesses. In this work, we describe the optical and electrical transport properties of an ultrathin Au granular film with an intentional thickness gradient for an in-depth study of the behavior near percolation.

An Au granular film with an intentional thickness gradient was deposited on an epi-polished *c*-axis oriented sapphire substrate (50 mm in diameter) by off-axis RF magnetron sputtering at an oblique angle of ~60° from the substrate normal. Physical and structural properties were measured along the thickness gradient. X-ray diffraction was done with a Panalytical Empyrean x-ray diffractometer with Cu K_α radiation in the Bragg–Brentano geometry. The optical properties were characterized by a Woollam VVASE vertical variable angle spectroscopic ellipsometer in the ultraviolet–visible–near infrared region 300–1700 nm (5880–33 333 cm^{-1}) with a 200 μm diameter spot size. The dc conductivity σ_{dc} was measured by the van der Pauw method with a Jandel four-point probe with 0.625 mm spacing and a Keithley source meter.

Diffraction results (figure 1) reveal peaks which can be assigned to the (111) and (222) orientations of fcc Au nanocrystallites. Since deposition was done from the gas phase, we assume that the nanocrystallite size is the relevant parameter in characterizing the film properties [37–40]. The nominal diameter d was

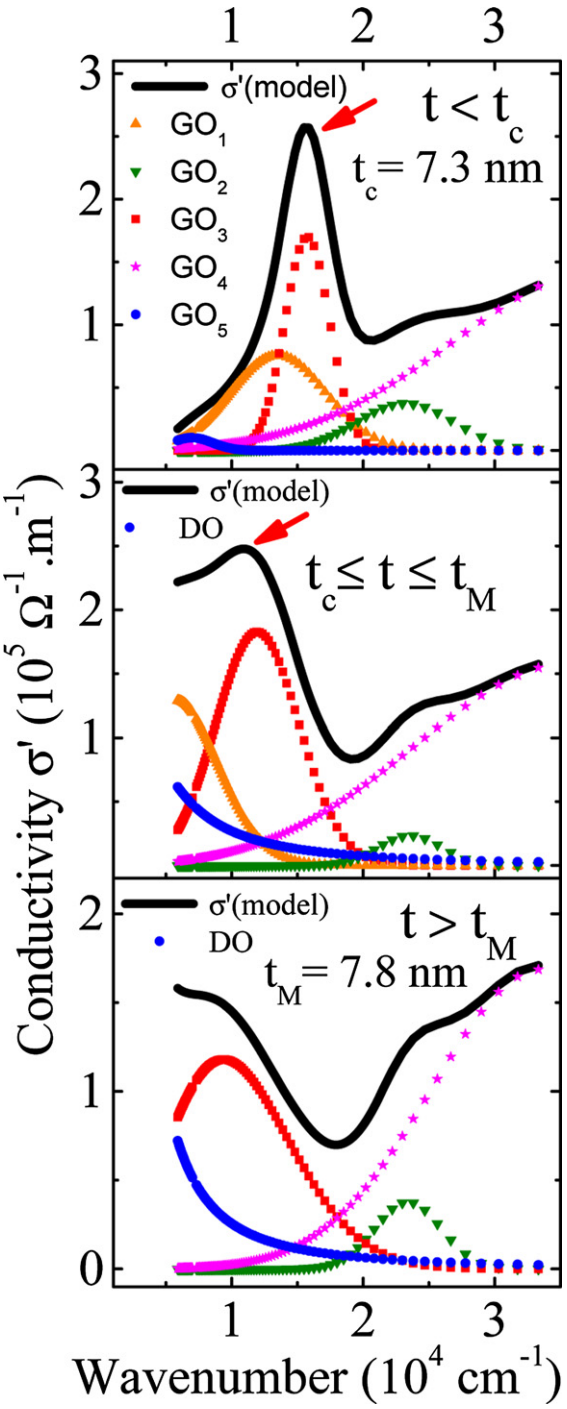

Figure 2. Frequency dependence of the optical conductivity. Symbols show the different Gaussian–Drude oscillators used to model the optical conductivity in the visible-near infrared region. At $t < t_c$, three oscillators (1, 2 and 3) are required to describe the LSPR contribution. With increasing thickness ($t_c \leqslant t \leqslant t_M$), oscillator 2 undergoes a gradual transformation to the Drude oscillator. Moreover, Gaussian oscillators 1 and 3 shift toward lower frequencies as t increases until Gaussian oscillator 3 disappears when $t > t_M$. In all cases, two additional Gaussian oscillators (4 and 5) are also required to describe the Au d electron interband transitions in the ultraviolet region. Plasmon resonances are indicated by red arrows.

estimated from the line broadening at half the maximum intensity of the diffraction peak based on the Scherrer equation with values ranging between 4.5 nm and 9.4 nm. The average gradient of 1.1 Å mm^{-1} was determined from a linear fit to the graph of the d values as a function of position (figure 1, inset).

To accurately evaluate the effective optical constants and thicknesses of the films, the incident angle independent pseudo-dielectric functions were fitted with a three-phase model (air/film/sapphire) including different combinations of a Drude oscillator and Gaussian oscillators, from which the complex dielectric

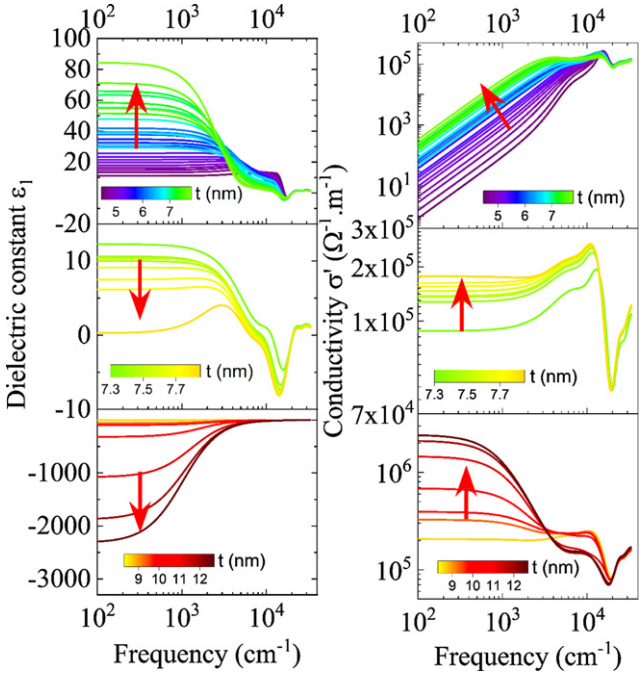

Figure 3. Dielectric constant and optical conductivity obtained from optical measurements for 4.9 nm $\leqslant t \leqslant$ 11.6 nm as indicated by the color maps. Top graphs correspond to $t < t_c = 7.3$ nm, bottom ones to $t > t_M = 7.8$ nm and those in the middle correspond to the percolation region ($t_c \leqslant t \leqslant t_M$). The arrows indicate increasing film thickness.

function $\hat{\varepsilon}(\omega)$ as a function of angular frequency ω was determined at each measured sample point:

$$\hat{\varepsilon}(\omega) = \varepsilon(\omega)_{\mathrm{DO}} + \sum_{n=1}^{N} \varepsilon_n(\omega)_{\mathrm{GO}} + \varepsilon_\infty \tag{4}$$

where $\varepsilon(\omega)_{\mathrm{DO}}$ is the complex dielectric function of a Drude oscillator, $\varepsilon_n(\omega)_{\mathrm{GO}}$ the complex dielectric function of the nth Gaussian oscillator obeying the Kramers–Kronig relationship, and ε_∞ the background dielectric constant. The model parameters (optical constants and thickness) were determined by minimizing the mean squared error.

Figure 2 shows the analyzed optical conductivity which can be broken into 3 regimes, depending on the thickness. All spectra display two features due to the Au d electron interband transitions in the ultraviolet region. For films thinner than t_c (figure 3(a)) there are three localized surface plasmon resonances, all of which can be modeled as Gaussian oscillators. As t increases toward t_c, one of the plasmon resonances shifts to lower frequency. At t_c it transforms into a Drude oscillator, the signature of a free-electron contribution to the conductivity, and it remains so for all larger thicknesses. With further increase in thickness, the two remaining plasmon resonances shift to lower frequency until one of the plasmon resonances disappears at the metal-to-dielectric transition which coincides with the change in sign of the dielectric constant (figure 4).

As shown in figure 3 (left panel), $\varepsilon_1(0)$ rose dramatically with increasing t as it approached $t_c = 7.3$ nm, and it then decreased for larger t values, reaching zero at $t_M = 7.8$ nm. From effective medium theory (EMT), one would have anticipated that in going from the dielectric to the metallic regimes, $\varepsilon_1(0)$ would continually decrease with increasing t, in stark contrast to the observations. However, EMT is inappropriate in the critical region as it predicts that sample morphology has a pronounced effect on the optical properties whereas percolation behavior is dependent only on dimensionality. Moreover, in the dielectric region, the nanograins tend to show self-order [2], and scattered fields may add coherently whereby EMT is again inappropriate as disorder is a necessary condition [41].

As predicted by classical percolation theory [24, 27, 42] $\varepsilon_1(0)$ (figure 4) obeys the scaling law of equation (1). While these results are similar to those Hövel *et al* [29, 30], the use of an insulating substrate removes any ambiguity surrounding substrate conduction [20] while the thickness gradient ensures that many measurements can be made, each with a high precision value for the thickness. The fitted value of $s \sim 1$ is in accord with the empirical values of the universal law for 3-D networks. The physical origin of the divergence remains unclear although one may postulate that it may be related to hot spots along the

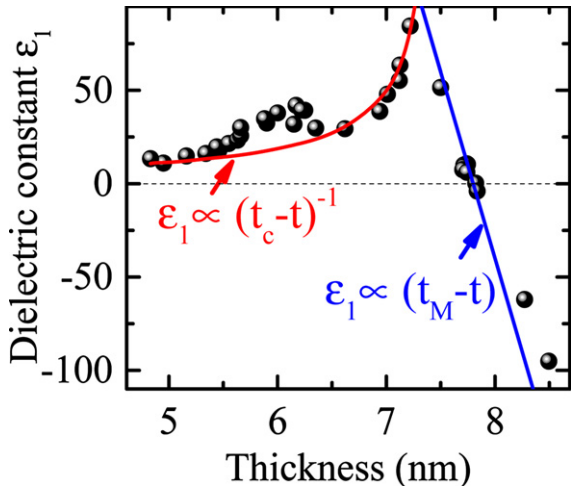

Figure 4. Real part of the static dielectric constant as a function of film thickness t. The solid red and black lines correspond to $\varepsilon_1(0) \propto (7.3\ \text{nm} - t)^{-1}$ and $\varepsilon_1(0) \propto (7.8\ \text{nm} - t)$, respectively.

percolative path where the electric field becomes greatly enhanced as seen in surface enhanced Raman scattering [43, 44].

For thicknesses greater than t_c, percolation theory [equation (2)] dictates that σ_{dc} follows scaling behavior. Near t_c, there is fluctuation in σ_{dc} (figure 5(a)) as might be expected near the percolation threshold. While σ_{dc} decreased by more than 4 orders of magnitude in a very narrow range for $t < t_c$, it deviates from the expected power law relationship because classical percolation theory does not account for TC which becomes more important as t approaches t_c.

To describe the behavior in the transition region between the dielectric and metallic regimes, we consider the importance of TC [45, 46]. Here we appeal to JUPL to describe the electronic transport in this transition region where $t_c < t < t_M$. According to JUPL,

$$\sigma'(\omega) \sim \sigma_{\text{dc}} + A\omega^n \tag{5}$$

where A is a constant and the exponent n (typically $0 < n < 1$) is related to the ratio of the competing electron tunneling/capacitive paths among nanoparticles. For the present case, $\sigma'(\omega)$ obeys the JUPL dependence just above the percolation threshold although the conduction mechanism is dominated by the fractal dimension of percolation clusters [45, 46] rather than well-isolated nanoparticles. Consequently, a combination of both metallic and thermally activated tunneling connections contribute to the conduction.

In order to describe the overall electrical conductivity film, we have considered a random-resistor network [23, 45] consisting of a regular array of cells. Let p denote the probability that two neighboring cells have metallic connections. Consequently, when the metallic cells are densely packed $p \to 1$, and conversely when the cells are isolated from one another $p \to 0$. Accordingly, percolation takes place at critical fraction p_c with $0 < p_c < 1$. To model the ac response, we make the following assumptions: the grains are connected in series by two types of elements, either by (i) metallic resistance R_M or (ii) a parallel combination of tunneling resistance R_t and effective capacitance C; and the nanoparticle size is dependent on the thickness but the resistances described by R_t are constant at a given thickness. The values of n found from fitting equation (4) to the measured $\sigma'(\omega)$ relate to the effective fraction of capacitive paths in the network involved in the *ac* conduction. Since there is an equal fraction of tunneling paths, the resulting exponents n (figure 5(b)) of 0.25 at t_c and 0.16 at t_M correspond to $p = 0.5$ and 0.78, respectively, consistent with the results on simulations of random R–C networks [47]. The JUPL regime disappears when the electrical conduction is dominated by electron transport along the meandering and ramified gold interconnected islands [20, 21] as seen in $\sigma'(\omega)$ (figure 3 bottom right).

In summary, we have measured optical constants of an ultrathin film of granular gold with a constant thickness gradient to provide unambiguous evidence of the divergence of the static dielectric constant at the percolation threshold. The dielectric constant be described by scaling laws according to the classical percolation theory while the static conductivity cannot due to the presence of tunneling conductivity. Importantly, for films slightly thicker than the critical thickness, the electronic transport follows Jonscher's universal power law while $\varepsilon_1(0)$ remains positive even though there is the Drude signature of free charge carriers. Only for larger thicknesses when $\varepsilon_1(0)$ changes sign does the conduction become metallic.

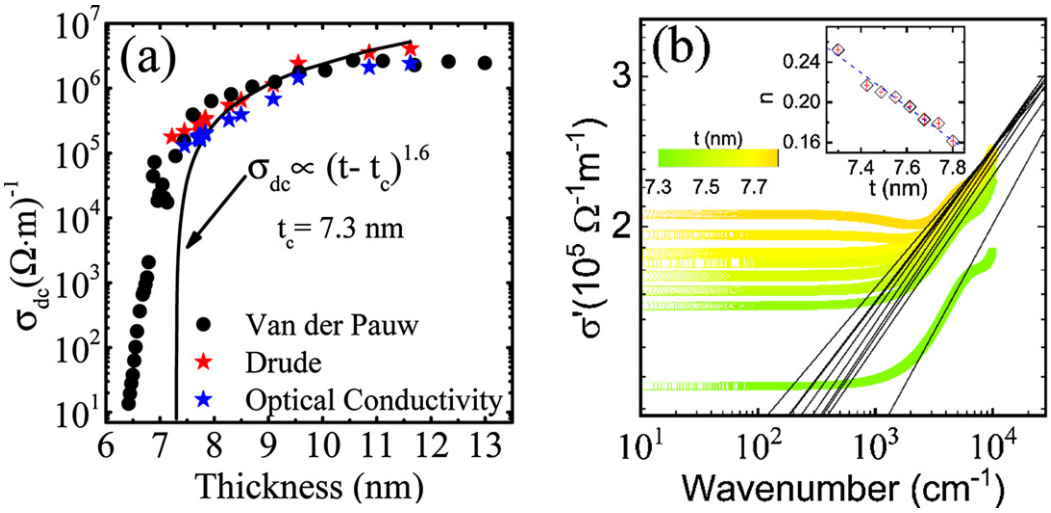

Figure 5. (a) dc resistivity measured with the van der Pauw method, determined from the Drude equation, and extrapolated from the optical conductivity (figure 3). The full line is the prediction by percolation theory. (b) Log–log plot of $\sigma'(\omega)$ as a function of angular frequency corresponding to the different thicknesses indicated by the color map. Solid lines indicate the fit of the data to a power law with the exponent values shown in the inset.

Acknowledgments

MD acknowledges financial support from Vicerrectorado de Politica Cientifica y Tecnologica (UCA) under grant AC2020-025.

ORCID iDs

H Bakkali https://orcid.org/0000-0001-7351-3948
E Blanco https://orcid.org/0000-0002-2234-1477
S E Lofland https://orcid.org/0000-0002-1024-5103
M Domínguez https://orcid.org/0000-0002-7889-7220

References

[1] Zhang H L, Evans S D and Henderson J R 2003 Spectroscopic ellipsometric evaluation of gold nanoparticle thin films fabricated using layer-by-layer self-assembly *Adv. Mater.* **15** 531–4
[2] Abeles B, Sheng P, Coutts M D and Arie Y 1975 Structural and electrical properties of granular metal films *Adv. Phys.* **24** 407–61
[3] Gittleman J I, Goldstein Y and Bozowski S 1972 Magnetic properties of granular nickel films *Phys. Rev.* B **5** 3609–21
[4] Cohen R W, Cody G D, Coutts M D and Abeles B 1973 Optical properties of granular silver and gold films *Phys. Rev.* B **8** 3689–701
[5] Bakkali H, Dominguez M, Batlle X and Labarta A 2016 Universality of the electrical transport in granular metals *Sci. Rep.* **6** 29676
[6] Bakkali H and Dominguez M 2013 Differential conductance of Pd-ZrO_2 thin granular films prepared by RF magnetron sputtering *Europhys. Lett.* **104** 17007
[7] Bakkali H, Blanco E, Dominguez M, de la Mora M B, Sánchez-Aké C and Villagrán-Muniz M 2017 Optical properties of Au–TiO_2 and Au–SiO granular metal thin films studied by spectroscopic ellipsometry *Appl. Surf. Sci.* **405** 240–6
[8] Bakkali H, Blanco E, Domínguez M and Garitaonandia J S 2017 Fabrication and optical properties of nanostructured plasmonic Al_2O_3/Au-Al_2O_3/Al_2O_3 metamaterials *Nanotechnology* **28** 335704
[9] Hu M-S, Chen H-L, Shen C-H, Hong L-S, Huang B-R, Chen K-H and Chen L-C 2006 Photosensitive gold-nanoparticle-embedded dielectric nanowires *Nat. Mater.* **5** 102–6
[10] Clavero C 2014 Plasmon-induced hot-electron generation at nanoparticle/metal-oxide interfaces for photovoltaic and photocatalytic devices *Nat. Photon.* **8** 95–103
[11] Bai G, Wu C, Jin J and Yan M 2016 Structural, electron transportation and magnetic behavior transition of metastable FeAlO granular films *Sci. Rep.* **6** 24410
[12] Zhang Y *et al* 2016 Self-assembled core–satellite gold nanoparticle networks for ultrasensitive detection of chiral molecules by recognition tunneling current *ACS Nano* **10** 5096–103
[13] Cha H, Yoon J H and Yoon S 2014 Probing quantum plasmon coupling using gold nanoparticle dimers with tunable interparticle distances down to the subnanometer range *ACS Nano* **8** 8554–63
[14] Qian H, Xiao Y and Liu Z 2016 Giant Kerr response of ultrathin gold films from quantum size effect *Nat. Commun.* **7** 13153
[15] Beloborodov I S, Lopatin A V, Vinokur V M and Efetov K B 2007 Granular electronic systems *Rev. Mod. Phys.* **79** 469–518
[16] Beloborodov I S, Efetov K B, Altland A and Hekking F W J 2001 Quantum interference and Coulomb interaction in arrays of tunnel junctions *Phys. Rev.* B **63** 115109

[17] Sheng P, Abeles B and Arie Y 1973 Hopping conductivity in granular metals *Phys. Rev. Lett.* **31** 44–7
[18] Batlle X and Labarta A 2002 Finite-size effects in fine particles: magnetic and transport properties *J. Phys. D: Appl. Phys.* **35** R15–42
[19] Mitani S, Takahashi S, Takanashi K, Yakushiji K, Maekawa S and Fujimori H 1998 Enhanced magnetoresistance in insulating granular systems: evidence for higher-order tunneling *Phys. Rev. Lett.* **81** 2799–802
[20] Yajadda M M A, Müller K H and Ostrikov K 2011 Effect of Coulomb blockade, gold resistance, and thermal expansion on the electrical resistance of ultrathin gold films *Phys. Rev.* B **84** 235431
[21] Wagner S and Pundt A 2008 Conduction mechanisms during the growth of Pd thin films: experiment and model *Phys. Rev.* B **78** 155131
[22] Jonscher A K 1977 The 'universal' dielectric response *Nature* **267** 673–9
[23] Kirkpatrick S 1973 Percolation and conduction *Rev. Mod. Phys.* **45** 574–88
[24] Efros A L and Shklovskii B I 1976 Critical behaviour of conductivity and dielectric constant near the metal-non-metal transition threshold *Phys. Status Solidi* B **76** 475–85
[25] Clerc J P, Giraud G, Laugier J M and Luck J M 1990 The electrical conductivity of binary disordered systems, percolation clusters, fractals and related models *Adv. Phys.* **39** 191–309
[26] Dubrov V E, Levinshtein M E and Shur M S 1976 Permittivity anomaly in metal-dielectric transitions. Theory and simulation *J. Exp. Theor. Phys.* **43** 1050–6
[27] Chou Y C and Jaw T-S 1988 Divergence of dielectric constant near the percolation threshold *Solid State Commun.* **67** 753–6
[28] van Dijk M A 1985 Dielectric study of percolation phenomena in a microemulsion *Phys. Rev. Lett.* **55** 1003–5
[29] Hövel M, Gompf B and Dressel M 2010 Dielectric properties of ultrathin metal films around the percolation threshold *Phys. Rev.* B **81** 035402
[30] Hövel M, Gompf B and Dressel M 2011 Electrodynamics of ultrathin gold films at the insulator-to-metal transition *Thin Solid Films* **519** 2955–8
[31] Isichenko M B 1992 Percolation, statistical topography, and transport in random media *Rev. Mod. Phys.* **64** 961–1043
[32] Shklovskii B I and Efros A L 1984 Percolation theory *Electronic Properties of Doped Semiconductors Springer Series in Solid-State Sciences* vol 45 (Berlin: Springer) pp 94–136
[33] Massey J G and Lee M 1996 Electron tunneling study of Coulomb correlations across the metal-insulator transition in Si:B *Phys. Rev. Lett.* **77** 3399–402
[34] Pakhomov A B, Wong S K, Yan X and Zhang X X 1998 Low-frequency divergence of the dielectric constant in metal-insulator nanocomposites with tunneling *Phys. Rev.* B **58** R13375–8
[35] Schwartzkopf M *et al* 2013 From atoms to layers: *in situ* gold cluster growth kinetics during sputter deposition *Nanoscale* **5** 5053–62
[36] Gensch M *et al* 2019 Correlating nanostructure, optical and electronic properties of nanogranular silver layers during polymer-template-assisted sputter deposition *ACS Appl. Mater. Interfaces* **11** 29416–26
[37] Barna P B and Adamik M 1998 Fundamental structure forming phenomena of polycrystalline films and the structure zone models *Thin Solid Films* **317** 27–33
[38] Yakubovsky D I, Arsenin A V, Stebunov Y V, Fedyanin D Y and Volkov V S 2017 Optical constants and structural properties of thin gold films *Opt. Express* **25** 25574
[39] Ma W G, Wang H D, Zhang X and Wang W 2010 Experiment study of the size effects on electron–phonon relaxation and electrical resistivity of polycrystalline thin gold films *J. Appl. Phys.* **108** 064308
[40] Mirigliano M, Borghi F, Podestà A, Antidormi A, Colombo L and Milani P 2019 Non-ohmic behavior and resistive switching of Au cluster-assembled films beyond the percolation threshold *Nanoscale Adv.* **1** 3119–30
[41] Aspnes D E 2011 Plasmonics and effective-medium theories *Thin Solid Films* **519** 2571–4
[42] Stauffer D and Aharony A 1992 *Introduction to Percolation Theory: Revised* 2nd edn (London: Taylor & Francis) https://doi.org/10.1201/9781315274386
[43] Grésillon S *et al* 1999 Experimental observation of localized optical excitations in random metal-dielectric films *Phys. Rev. Lett.* **82** 4520–3
[44] Santoro G *et al* 2014 Silver substrates for surface enhanced Raman scattering: correlation between nanostructure and Raman scattering enhancement *Appl. Phys. Lett.* **104** 243107
[45] Mantese J V, Curtin W A and Webb W W 1986 Two-component model for the resistivity and noise of tunneling metal-insulator composites *Phys. Rev.* B **33** 7897–901
[46] Toker D, Azulay D, Shimoni N, Balberg I and Millo O 2003 Tunneling and percolation in metal-insulator composite materials *Phys. Rev.* B **68** 041403
[47] Vainas B, Almond D P, Luo J and Stevens R 1999 An evaluation of random R–C networks for modelling the bulk ac electrical response of ionic conductors *Solid State Ion.* **126** 65–80